Received: 6 July 2018 | Revised: 24 October 2018 | Accepted: 25 October 2018

DOI: 10.1002/mrm.27614

FULL PAPER

Magnetic Resonance in Medicine

Robust kidney perfusion mapping in pediatric chronic kidney disease using single-shot 3D-GRASE ASL with optimized retrospective motion correction

Fabio Nery[1] | **Enrico De Vita**[2] | **Chris A. Clark**[1] | **Isky Gordon**[1] | **David L. Thomas**[3,4]

[1]Developmental Imaging and Biophysics Section, University College London Great Ormond Street Institute of Child Health, London, United Kingdom

[2]Department of Biomedical Engineering, School of Biomedical Engineering & Imaging Sciences, King's College London, King's Health Partners, St Thomas' Hospital, London, United Kingdom

[3]Department of Brain Repair and Rehabilitation, University College London Queen Square Institute of Neurology, Queen Square, London, United Kingdom

[4]Leonard Wolfson Experimental Neurology Centre, University College London Queen Square Institute of Neurology, Queen Square, London, United Kingdom

Correspondence
Fabio Nery, Developmental Imaging and Biophysics Section, University College London Great Ormond Street Institute of Child Health, London WC1N 1EH, United Kingdom.
Email: fabio.nery.13@ucl.ac.uk

Funding information
Kidney Research UK, Grant/Award Number: ST1/2013; NIHR Great Ormond Street Hospital Biomedical Research Centre; UCL Leonard Wolfson Experimental Neurology Centre, Grant/Award Number: PR/ylr/18575

Purpose: To develop a robust renal arterial spin labeling (ASL) acquisition and processing strategy for mapping renal blood flow (RBF) in a pediatric cohort with severe kidney disease.

Methods: A single-shot background-suppressed 3D gradient and spin-echo (GRASE) flow-sensitive alternating inversion recovery (FAIR) ASL acquisition method was used to perform 2 studies. First, an evaluation of the feasibility of single-shot 3D-GRASE and retrospective noise reduction methods was performed in healthy volunteers. Second, a pediatric cohort with severe chronic kidney disease underwent single-shot 3D-GRASE FAIR ASL and RBF was quantified following several retrospective motion correction pipelines, including image registration and threshold-free weighted averaging. The effect of motion correction on the fit errors of saturation recovery (SR) images (required for RBF quantification) and on the perfusion-weighted image (PWI) temporal signal-to-noise ratio (tSNR) was evaluated, as well as the intra- and inter-session repeatability of renal longitudinal relaxation time (T_1) and RBF.

Results: The mean cortical and/or functional renal parenchyma RBF in healthy volunteers and CKD patients was 295 ± 97 and 95 ± 47 mL/100 g/min, respectively. Motion-correction reduced image artefacts in both T_1 and RBF maps, significantly reduced SR fit errors, significantly increased the PWI tSNR and improved the improved the repeatability of T_1 and RBF in the pediatric patient cohort.

Conclusion: Single-shot 3D-GRASE ASL combined with retrospective motion correction enabled repeatable non-invasive RBF mapping in the first pediatric cohort with severe kidney disease undergoing ASL scans.

KEYWORDS
arterial spin labeling (ASL), kidneys, motion correction, pediatric MRI, renal blood flow, renal MRI

1 | INTRODUCTION

Arterial spin labeling (ASL) is a quantitative MRI technique, unique in its ability to quantify tissue perfusion in vivo completely non-invasively by using the subjects' own blood as an endogenous contrast agent.[1,2] More than 2 decades of technical developments have established ASL as a valuable tool in neuroimaging, and more recently enabled its initial translation to the clinic.[3] In addition, ASL can be used to assess perfusion in other organs of the body.[4-6] Renal ASL holds great potential, given that it provides quantification of a crucial pathophysiological parameter of kidney disease: renal blood flow (RBF). Furthermore, it achieves this without requiring injection of MR contrast agents, which are typically contraindicated for patients with impaired renal function.[7] RBF differences in chronic kidney disease (CKD) and acute kidney injury patients have been demonstrated with ASL when compared to healthy volunteers,[8-12] as well as age-related variations in kidney perfusion.[11,13] ASL has also been used to quantify and monitor perfusion of renal allografts[14-16] and healthy adult kidney donors.[17] Changes in RBF following therapeutic interventions have also been investigated.[16,18]

The unique features of ASL (not requiring the administration of contrast agents or having an associated radiation burden) make it a very attractive technique for pediatric applications where ensuring a safe and tolerable scanning experience is of crucial importance. Nevertheless, renal ASL is a challenging technique[19] and so far has remained confined to specialist centers and adult populations in the absence of widespread clinical uptake. This work focuses on addressing one of the main challenges associated with performing renal ASL, namely subject motion, either because of respiration or bulk patient movement, with the goal of achieving an ASL protocol that can robustly be used in the clinic, particularly in pediatric cohorts. Artefacts in ASL RBF maps can originate from kidney movement at different stages of the ASL pipeline: (1) motion artefacts in the acquired control and/or label images (particularly in multi-shot acquisitions), (2) control-tag subtraction errors, (3) inconsistent position of the kidneys in the perfusion-weighted image (PWI) time series, (4) misalignment between ASL and "calibration" reference images (M_0 and/or T_1 maps), and (5) artefacts in the calibration images (e.g., errors in the T_1 maps because of movement during the T_1 mapping acquisition) that propagate into the RBF maps. All these issues are addressed in this work by combining a motion-robust image readout with an optimized retrospective motion correction (MC) pipeline that uses image registration and weighted-averaging to reduce the deleterious effects of corrupted ASL PWIs. The proposed methods were tested in a small group of adult healthy volunteers and a pediatric cohort with severe kidney disease, the first time such a patient group has undergone renal ASL imaging to our knowledge. Image quality metrics and intra- and inter-session T_1 and RBF repeatability analyses were used to evaluate the effectiveness of the proposed MC approaches and the feasibility of renal ASL in the patient cohort.

2 | METHODS

Two separate in vivo MRI studies were performed to investigate the feasibility of renal ASL. The first consisted of a preliminary demonstration of renal ASL using a motion-robust readout (single-shot 3D gradient and spin-echo [3D-GRASE]) and evaluated retrospective noise reduction methods in healthy volunteers. In the brain, 3D-GRASE ASL is typically implemented as a multi-shot acquisition.[3] Renal ASL using a segmented 3D readout was first shown in healthy volunteers in Cutajar et al.[20] Using segmented 3D fast spin-echo, Robson et al.[21] optimized a renal ASL protocol for single-kidney lesion detectability. However, scan time was relatively long (~15 min for both kidneys including M_0 acquisition) and relied on a timed-breathing strategy for optimal image quality. For renal imaging in a pediatric population, our initial experience indicated that a multi-shot approach would not be practical because of the high likelihood of patient movement in such a cohort. We therefore opted for a less demanding acquisition protocol (from the patients' perspective) with a shorter scan time and no need for synchronized breathing, using a single-shot acquisition, which is much more robust to motion. Readout parameters were chosen such that a short echo train duration (ETD) was achieved. Although this imposes limits on the achievable spatial resolution, it ensures that (1) intra-shot motion may be assumed to be negligible, and (2) excessive blurring because of T_2 decay during the echo-train, which decreases the effective resolution of the scans, can be avoided. Single-shot acquisitions also enable short scan times, even when acquiring a large number of ASL control-label pairs. The second study assessed the repeatability of renal ASL in a pediatric cohort with severe CKD using the same readout and an optimized retrospective MC pipeline.

2.1 | MR acquisition

MR data from 16 subjects was acquired on a Siemens Avanto 1.5T scanner (Siemens Healthcare, Erlangen, Germany), using the spine and body matrix coils. This study was approved by the ethics board of the NHS and the UCL Great Ormond Street Institute of Child Health ethics committee. The renal ASL protocol consisted of a single-shot flow-sensitive alternating inversion recovery (FAIR),[22,23] Q2TIPS[24] 3D-GRASE pulse sequence with background suppression.[25,26] Two background suppression pulses were used as per the scheme described in Günther et al.[25] Slab-selective pre-labeling WET saturation pulses[27] and a single post-labeling sinc saturation

pulse were used. Respiratory triggering (RT) was used to trigger the ASL inversion pulses at end-expiration (threshold = 20%, delay = 0 s). Other parameters include: FOV = 288 × 288 × 60 mm^3, voxel size = 4.5 × 4.5 × 6 mm^3, TR/TE = 3000/31.5 ms; bandwidth = 2790 Hz/pixel; centric partition ordering; echo-spacing = 0.4 ms; partial Fourier factor = 3/4 along the partition direction (anterior → posterior); ETD = 248 ms, phase-encoding direction = left → right, ASL inflow time (TI) = 1200 ms, bolus duration (TI1) = 900 ms.[24] Arm radiofrequency shields were used to avoid phase wrap-around artefacts (Accusorb MRI, MWT Materials, NJ). Spectral fat saturation was used. The number of control-tag pairs acquired was 15 in healthy volunteer scans and 25 in patient scans, for a corresponding nominal scan time (i.e., excluding delays because of RT) of 90 and 150 s, respectively. Important features of the acquisition that were prioritized during protocol setup were high SNR with reduced sensitivity to motion, hence the choice for a 3D single-shot, single-TI acquisition at moderate resolution with a considerable number of ASL pairs. In patient scans, 2 ASL runs were acquired with an ~30 min gap between acquisitions for an intra-session reproducibility assessment. Between the 2 runs, the patients remained inside the scanner for additional MR scans. A separate reference proton-density (PD)-weighted scan (1 average) with similar parameters (but without any inversion or saturation pulses) was acquired to enable conversion of the PWI signal to absolute RBF. A trigger delay of 1200 ms (matching the TI of the ASL scans) was implemented to ensure the PD volumes were acquired at the same point in the respiratory cycle as the ASL data, to minimize misregistration.

2.2 | Study 1: feasibility and noise reduction of renal ASL in healthy volunteers

Five healthy adult volunteers (age [y] = 32 ± 5 [mean ± SD], range = 26–37; 3 male) underwent 2 ASL runs. In run 1, the volunteers were asked to remain still and breathe normally ("still" condition). One volunteer underwent 2 additional scans in the "still" condition 7 and 21 d after the first scan to assess the repeatability of RBF. In run 2, volunteers were asked to alter their respiratory rate and amplitude during the scan (by means of an audible cue), to reduce the efficacy of RT and introduce kidney position inconsistencies between control and tag images ("movement" condition). Retrospective MC methods were then tested to reduce the contribution of the corrupted measurements to the final (averaged) ASL PWI.

2.2.1 | Reducing the contribution of corrupted ASL measurements

Several approaches have been proposed to reduce the contribution of corrupted ASL PWIs to the average PWI subsequently used for perfusion quantification.[28-30] A possible strategy is to weight the contribution of individual PWIs differently according to "noise" estimates derived from the ASL data itself. In general, if ϵ_p is a vector of noise estimates for each measurement (e.g., an ASL PWI), the vector of weights can be obtained by:

$$w_p = \frac{1}{c\epsilon_p}, \tag{1}$$

where

$$c = \sum_{p=1}^{N} \frac{1}{\epsilon_p}, \tag{2}$$

and N is the number of measurements. As such

$$\sum_{p=1}^{N} w_p = 1. \tag{3}$$

The weighted mean PWI ($\bar{I}$) is given by

$$\bar{I} = \sum_{p=1}^{N} w_p \cdot I_p, \tag{4}$$

where I_p is the PWI corresponding to control-tag pair p. Two strategies for computing the vector of noise estimates ϵ_p were explored in this study (ϵ_p^{DVARS} and ϵ_p^{MVARS})

$$\epsilon_p^{DVARS} = \frac{1}{M} \sum_{r=1}^{M} \left\{ \left[I_p(r) - I_{p-1}(r) \right]^2 + \left[I_{p+1}(r) - I_p(r) \right]^2 \right\}, \tag{5}$$

$$\epsilon_p^{MVARS} = \frac{1}{M} \sum_{r=1}^{M} \left\{ \left[I_p(r) - I_{mean}(r) \right]^2 \right\}, \tag{6}$$

where $I_p(r)$ and $I_{mean}(r)$ correspond, respectively, to the intensity of the PWI resulting from the ASL pair p and a mean (averaged) PWI over all pairs, at locations (voxels) r. The total number of voxels over which the noise metric is calculated is M.

The first approach (that uses ϵ_p^{DVARS} as the weighting factor), henceforth known as $wMean^{DVARS}$, has been proposed in a previous ASL study in the brain.[30] ϵ_p^{DVARS} is only defined if temporally adjacent measurements exist, leading to rejection of the first and last PWIs regardless of whether they are corrupted by artefacts. We propose an alternative approach, using ϵ_p^{MVARS} (henceforth known as $wMean^{MVARS}$; M referring to the mean PWI), which requires no data rejection. This is particularly important for ASL protocols where the number of averages is low (e.g., multi-TI studies) as avoiding the rejection of uncorrupted data is essential to maximize scan efficiency and perfusion SNR. Furthermore, this allows ϵ_p^{MVARS}

TABLE 1 Summary of implemented noise-reduction methods

Method	Name	Noise estimate	Mask	No. of iterations
1	$wMean^{DVARS}$	ϵ_p^{DVARS}	none	1
2	$wMean_{masked}^{DVARS}$	ϵ_p^{DVARS}	cortex	1
3	$wMean^{MVARS}$	ϵ_p^{MVARS}	none	10[a]
4	$wMean_{masked}^{MVARS}$	ϵ_p^{MVARS}	cortex	10[a]

[a]Tests during the implementation stage suggest that for our data sets $wMean^{MVARS}$ converges (i.e., negligible change in individual weights across iterations) after a small number of iterations (<10) (see Supporting Information Figure S3).

to be iteratively calculated. In the first iteration, I_{mean} corresponds to a standard mean PWI. In subsequent iterations, I_{mean} corresponds to the (improved) weighted mean image from the previous iteration. Both approaches allow the regions (voxels) over which the noise estimates are calculated to be specified. For both $wMean^{DVARS}$ and $wMean^{MVARS}$, the vector of noise weights was computed using voxels (1) from the entire FOV, and (2) restricted to the renal cortex. In summary, 4 combinations of noise reduction methods were tested (see Table 1).

Two metrics were used to quantitatively evaluate the effect of the weighted averaging methods: cortical tSNR ($tSNR_{ctx}$) and volumetric image entropy (H_{vol}). The calculation of tSNR was restricted to cortical voxels to better reflect the expected effect of the noise suppression methods on the actual perfusion estimates. Image entropy was calculated as a proxy of image quality over the entire FOV, as minimization of image entropy has been associated with a reduction in image blurring[31] (a prevalent artefact in ASL when multiple PWIs in inconsistent positions are averaged). These are respectively defined as $tSNR_{ctx} = \bar{I}_{ctx}/\sigma_{ctx}^t$ and $H_{vol} = -\sum_{b=1}^{B} p_b log_2 p_b$, where $\bar{I}_{ctx}$ is the (weighted) mean PWI signal in a cortical voxel, σ_{ctx}^t is the SD of the PWI signal time series in a cortical voxel, B is the number of bins for entropy calculation ($B = 256$ in this study), and p_b is the normalised intensity histogram count (probability) at bin b. For the evaluation of the weighted averaging methods, σ_{ctx}^t is calculated as the weighted SD using the resulting vector of weights w_p, which for a vector x with elements $x_1, x_2, \ldots, x_N$ and using weights $w_1, w_2, \ldots, w_N$ is defined as

$$\sigma_x^w = \sqrt{\frac{\sum_{i=1}^{N} w_i \left(x_i - \bar{x}\right)^2}{\sum_{i=1}^{N} w_i}}, \tag{7}$$

where $\bar{x}$ is the weighted mean of x. Results, where presented in numeric form, are expressed as mean ± SD considering all voxels within the cortical ROI. Two-tailed paired t-tests were used to assess for statistically significant differences in each of the metrics after applying each MC method when compared to the "No correction" condition. The threshold for statistical significance was $P < 0.05$.

2.3 | Study 2: feasibility of renal ASL in a pediatric cohort with CKD using an optimized retrospective motion correction pipeline

Eleven children (age [y]: 12 ± 3 (mean ± SD), range: 7–17; 8 male) with severe CKD (estimated glomerular filtration rate [eGFR] (mL/min per 1.73 m^2) = 26 ± 9 [mean ± SD], range = 12–47) underwent 2 separate scan sessions on different days to assess the intra- and inter-session reproducibility of the RBF measurements using an identical ASL protocol to that used in study 1. The time between scan sessions (days) was: 23 ± 10 (mean ± SD, range: 7–35). Because changes in T_1, a required parameter for ASL quantification, have been associated with renal impairment,[32,33] patient scans included acquisition of saturation recovery (SR) 3D-GRASE time series for T_1 mapping on a subject-by-subject basis with parameters matched to the accompanying ASL readout module and 9 post-saturation delays (range = 100−2500 ms; increment = 300 ms). These were repeated up to 3 times in each session (dependent on patient tolerance) that across all patients resulted in a total of 52 SR data sets (2 excluded because of extreme motion). Given that the likelihood of movement increases when scanning children, the effect of retrospective MC strategies on the intra- and inter-session reproducibility of the T_1 and RBF measurements was assessed.

2.3.1 | Retrospective motion correction pipeline

Retrospective MC methods used in this work included 3D rigid body image registration as well as $wMean_{masked}^{MVARS}$. The choice of rigid body registration is consistent with previous renal ASL studies[8,16,34-36] and was based on several factors: (1) only intra-subject registrations were performed, and (2) reduced static tissue signal in background suppressed ASL renders highly complex transformations such as those required for non-rigid deformations challenging. All registrations were performed separately for the left and/or right kidneys to account for any independent movement.[37,38] In summary, 3 ASL processing pipelines were evaluated: A,

no MC; B, MC using image registration only; and C, MC using image registration combined with weighted averaging. In pipelines B and C, all volumes in the SR time series were registered to the non-background suppressed reference PD-weighted volume. All MC pipelines used the open-source *elastix* toolbox[39] to perform image registration. A mutual information similarity metric[40] was used to account for changes in intensity distributions between the various images. Optimization was performed using a stochastic gradient descent approach[41] (500 iterations). Diagrams detailing pipelines B and C are shown in Figure 1.

2.3.2 | Evaluating the impact of retrospective motion correction

Saturation recovery

The impact of image registration on the intra- and inter-session repeatability of the T_1 estimates was evaluated using the intra-class correlation coefficient (ICC) and the within-subject coefficient of variation (WSCV). Furthermore, the quality of the underlying SR fits obtained before and/or after image registration was assessed employing the root mean-squared error as a goodness-of-fit metric.

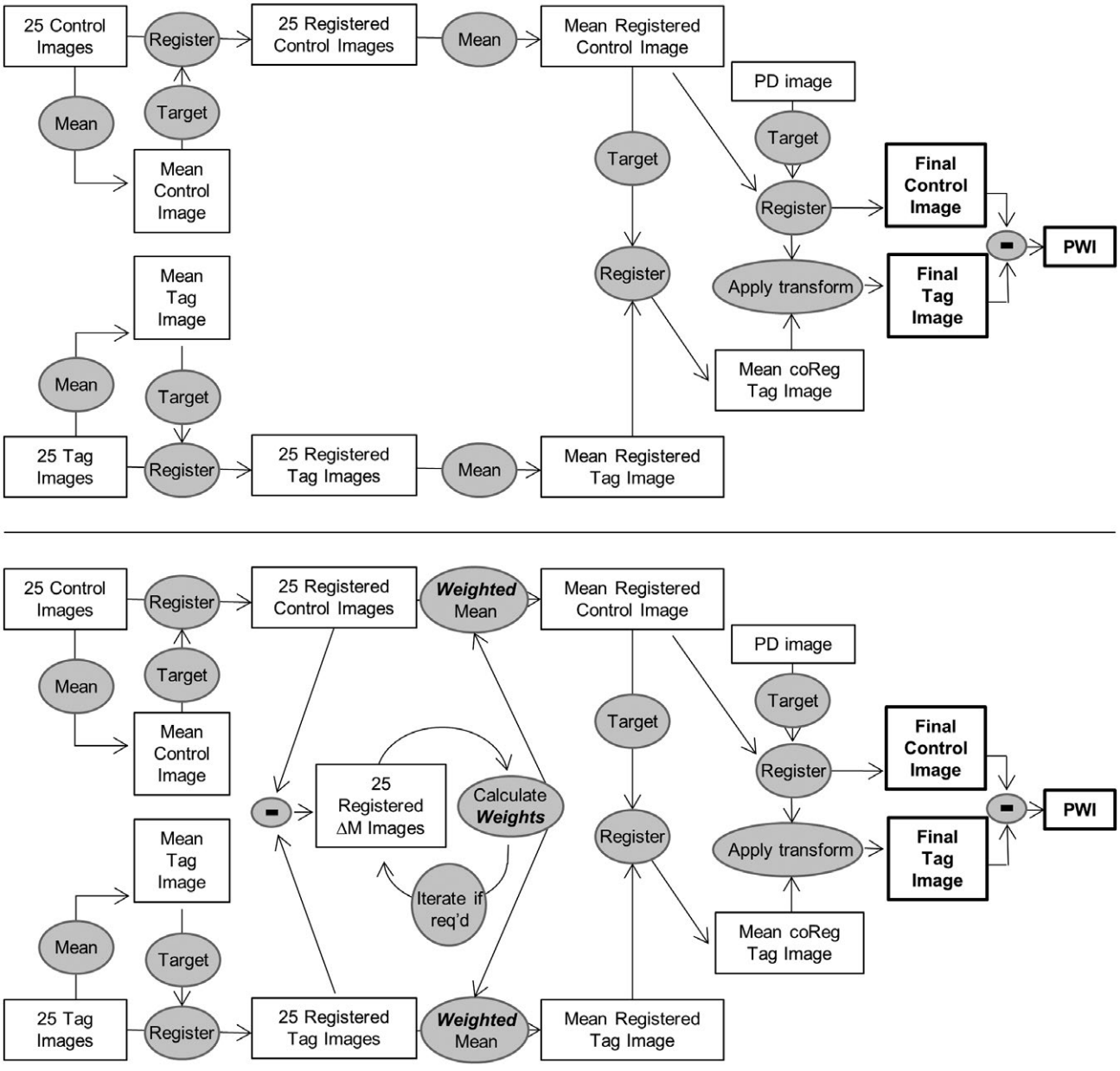

FIGURE 1 Motion correction (MC) pipelines for ASL data. Top: processing pipeline B. Bottom: processing pipeline C (note that processing pipeline A corresponds to the "no MC" case and therefore is not shown in this figure). The main difference between the two is that in pipeline C, weighted averaging was performed using the $wMean^{MVARS}_{masked}$ method. Note that in these diagrams, images or image series are referred to within rectangular boxes, whereas operations acting on images are enclosed in elliptical boxes

ASL

ICC and WSCV were also used to evaluate the intra- and inter-session repeatability of RBF. The effect of registration on the variability of the PWI signal was assessed by calculating the tSNR of the PWI time series in the functional renal parenchyma regions of interest (ROIs). A total translational motion index, Euclidean distance (ED),[42] was calculated as the square root of the sum of the squared displacements relative to the reference image (obtained from the transformation matrices output from the registration steps) to summarize the amount of kidney movement during the acquisition of the ASL data for each patient. This metric was used to capture the predominantly craniocaudal kidney displacements induced by respiration. The correlation between tSNR improvement, as well as age of the subjects and the ED in the corresponding scans, was assessed.

2.4 | Image analysis

For study 1 (healthy volunteers), perfusion quantification was performed using a single-compartment model[43] assuming a T_1 value for the kidney cortex of 0.966 s.[44] No image registration methods were used to align the data from the healthy volunteers, as the reduced bulk body movement combined with RT were sufficient to avoid motion artefacts in the still condition. Nevertheless, the M_0 value used for quantification was the median M_0 in whole-kidney ROIs (as shown in Figure 2B), obtained from a separate non-background suppressed 3D-GRASE reference scan. This ensures that in the case of the ASL and the M_0 data being misaligned, perfusion quantification values close to the boundaries of the kidney (i.e., in the cortex) will not be biased by using M_0 values from tissue outside the kidneys. Renal cortical ROIs were manually drawn in the reference non-background suppressed data. Average cortical perfusion values were calculated within these ROIs in each of the subjects.

For study 2 (pediatric CKD cohort), before computing the RBF maps, all ASL data was processed with the 3 MC pipelines described above. The same single-compartment quantification model was used to compute RBF values, but the additional MC methods applied to patient data allowed voxelwise M_0 values to be used. Furthermore, subject-specific

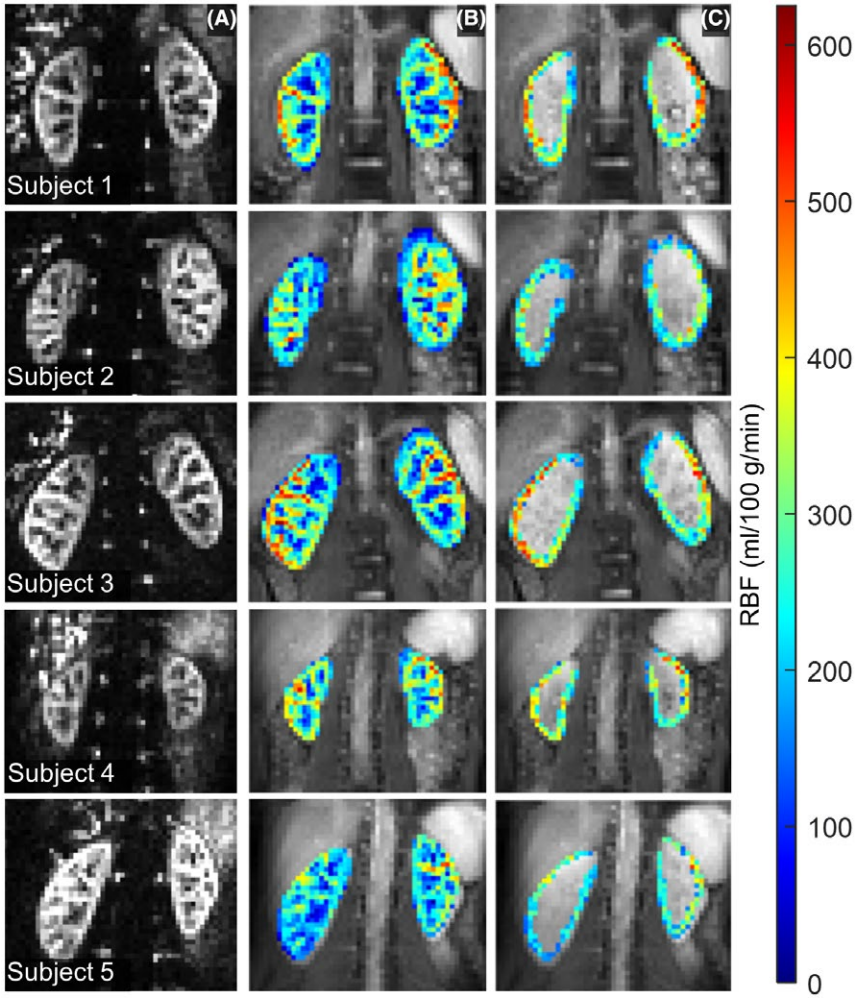

FIGURE 2 PWIs (A) and perfusion maps for the 5 healthy volunteers in this study. Whole-kidney (B) and cortex (C) perfusion maps are shown. The whole-kidney and cortical ROI was obtained by manual segmentation

voxelwise T_1 estimates were used to account for changes in tissue T_1 expected in CKD patients using fits of the SR data to a monoexponential recovery curve. ROIs were manually drawn on the PD-weighted images for calculating ROI-based statistics related to the quantitative MR measures. In patient data, the aim was to select all voxels deemed part of the functional renal parenchyma, with care not to include high intensity regions corresponding to a dilated collecting system or cysts. We opted to draw ROIs on the reference PD images to avoid biases related to drawing ROIs on PWIs in impaired kidneys, such as failing to include anatomically present cortex which is undetectable in the PWIs because of reduced perfusion. All ROIs were drawn by 1 author with 3+ y of experience in renal ASL and reviewed by 1 author who is a radiologist with 35 y of experience in renal imaging.

3 | RESULTS

3.1 | Study 1: Feasibility and noise reduction of renal ASL in healthy volunteers

3.1.1 | Perfusion quantification in the still condition

Healthy volunteer ASL scans in the "still" condition were free of motion artefacts (see Figure 2). Good image quality was obtained in a short nominal scan time (90 s) with clear cortico-medullary differentiation reflecting expected regional RBF differences. The mean cortical RBF across all subjects/scans was 295 ± 97 mL/100 g/min (range = 245–343 mL/100 g/min), within the range of RBF values obtained in healthy volunteers in previous studies (ranging from 139 ± 38 to 427 ± 20 mL/100 g/min).[13,45] The coefficient of variation of the mean RBF for volunteer 3 (see Figure 2), who underwent ASL scanning on 3 different days was 5.9%.

3.1.2 | Evaluation of noise reduction methods in healthy volunteers

All motion-correction methods reduced the effect of the corrupted measurements to the final PWI, albeit to a different extent. A statistically significant increase in $tSNR_{ctx}$ was found between the "No correction" condition and the $wMean^{MVARS}$ method (with and without cortical masking), demonstrating its effectiveness in reducing the PW signal variability across the ASL time series. Down-weighting individual corrupted PWIs significantly reduces blurring artefacts in the averaged PWI, improving the cortico–edullary differentiation particularly in heavily corrupted data (e.g., subject 4) (see Figure 3 and Supporting Information Figure S2). RT was effective in subject 3 even after instructing the subject to alter the respiratory rate, resulting in artefact-free data with standard averaging. Identical image quality after weighted averaging in this subject suggests that application of this method has no detrimental effects on high-quality data (see Supporting Information Figure S1). The image entropy (H_{vol}) decreased following all weighted averaging methods, reflecting the reduction of blurring in the resulting averaged PWI, with a statistically significant decrease in the case of $wMean^{MVARS}_{masked}$ when subject 3 is not included in the analysis. Table 2 summarizes the absolute values of $tSNR_{ctx}$ and H_{vol} averaged across all subjects. Individual PWIs from subject 1, as well as their corresponding weights determined with $wMean^{MVARS}_{masked}$, are shown in Figure 4. Measurements 11–15 show prominent motion artefacts resulting from the kidneys (and adjacent organs) changing position between control and/

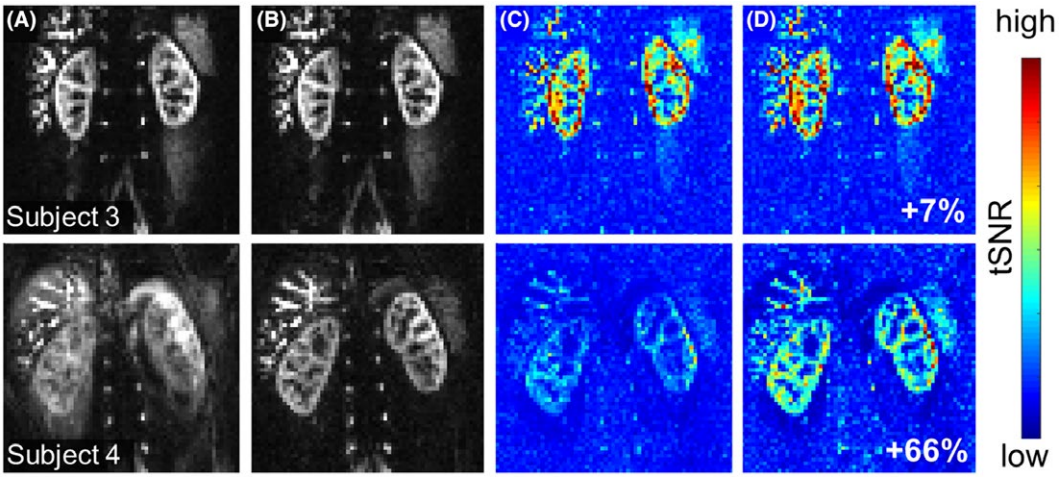

FIGURE 3 Averaged PWIs and voxelwise tSNR maps before and/or after noise-correction using $wMean^{MVARS}_{masked}$. Column A: mean PWI before correction. Column B: mean PWI after correction. Column C: voxelwise tSNR map before correction. Column D: voxelwise tSNR map after correction. The values in tSNR maps correspond to the mean increase in this metric in the cortical ROI when compared to the "No correction" case. See Supporting Information Figure S2 for results in remaining subjects

TABLE 2 Image quality metrics before and/ or after each proposed noise suppression methods (mean ± SD)

	All subjects				Subject 3 excluded			
	tSNR	P^a	H_{vol}	P^a	tSNR	P^a	H_{vol}	P^a
No correction	3.46 ± 1.55		5.33 ± 0.37		2.77 ± 0.22		5.39 ± 0.39	
$wMean^{DVARS}$	3.95 ± 1.33	0.074	5.02 ± 0.23	0.097	3.38 ± 0.47	0.063	4.99 ± 0.25	0.065
$wMean^{DVARS}_{masked}$	4.09 ± 1.37	0.061	5.00 ± 0.27	0.110	3.53 ± 0.64	0.068	4.97 ± 0.29	0.082
$wMean^{MVARS}$	4.18 ± 1.32	0.040[b]	4.85 ± 0.17	0.069	3.62 ± 0.50	0.048[b]	4.79 ± 0.13	0.058
$wMean^{MVARS}_{masked}$	4.50 ± 1.29	0.016[b]	4.83 ± 0.21	0.062	3.96 ± 0.54	0.022[b]	4.76 ± 0.17	0.049[b]

For $tSNR_{ctx}$ (calculated on a voxelwise basis), first the mean and SD of the metric values within the ROI are computed for each subject. The values in the table correspond to the mean across the subjects of the mean and SD within their corresponding ROIs. The values of H_{vol} correspond to the mean ± SD across subjects of the entropy calculated across the entire image volume. Data also shown for the case where subject 3 is excluded as the data from this subject is free of movement artefacts even before applying the proposed noise suppression methods, therefore the effect of noise suppression is negligible in this subject.

[a]Probabilities associated with the two-tailed paired t-tests to assess for statistically significant differences in the image quality metrics between "No correction" and the weighted averaging methods.

[b]Significant differences.

or label conditions. The contribution of this set of corrupted images to the averaged PWI is ~1 order of magnitude lower when using $wMean^{MVARS}_{masked}$ compared to standard averaging (3.5% vs. ≈33% [5/15]).

3.2 | Study 2: Feasibility of renal ASL in a pediatric cohort with CKD using an optimized retrospective motion correction pipeline

3.2.1 | Evaluating the impact of retrospective motion correction

T_1 measurements

Across the entire cohort (all patients/days/runs, $N = 50$ SR acquisitions), the cortical T_1 was found to be 1.89 ± 0.29 s (mean ± SD), range = 1.40–3.02 s without MC, which significantly decreased to 1.65 ± 0.21 s (mean ± SD), range = 1.26–2.14 s (two-tailed paired t-test $P < 0.00001$) after MC. This suggests that in the presence of uncorrected renal movement the T_1 estimates suffered from a significant positive bias. This can be problematic especially as increases in T_1 have been associated with presence of kidney disease.[32,33] Without MC, the WSCV and ICC were, respectively 12.3% and 0.085 (intra-session) and 13.0% and 0.254 (inter-session). With MC, the WSCV decreased (i.e., improved) to 6.5% (intra-session) and 7.4% (inter-session), and the ICC increased (i.e., improved) to 0.750 (intra-session) and 0.614 (intra-session). The RMS error of the SR fits was significantly lower using MC compared to without MC (paired t-test $P < 1e{-}10$).

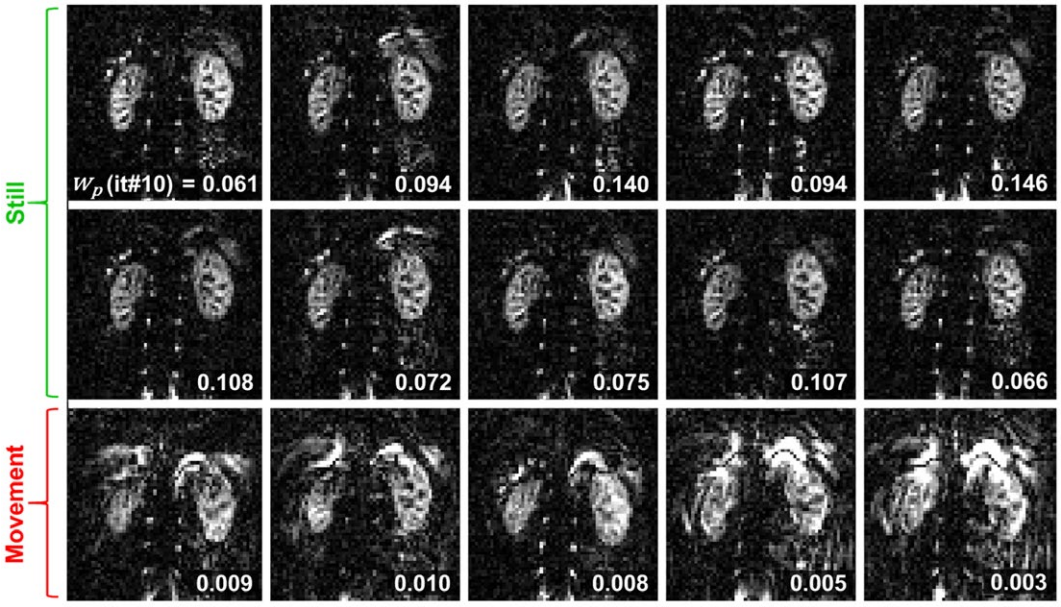

FIGURE 4 Effect of using $wMean^{MVARS}_{masked}$ on the contribution of each PWI (before averaging) to the mean PWI (subject 1). Individual PWIs (before averaging) shown together with corresponding weights (W_p) as determined by $wMean^{MVARS}_{masked}$

Background-suppressed ASL time series

Out of 44 possible ASL runs (11 children × 2 d/child × 2 runs/d), 1 was excluded because of the presence of artefacts unrelated to patient movement and 1 was excluded because of RT failure. The latter was caused by extreme bulk movement that resulted in the respiratory bellows shifting to a position where they were unable to record an accurate respiratory trace. Therefore, 42 ASL runs were analyzed. The mean increase in tSNR after applying pipelines B and C, relative to A was, respectively 19.2 ± 15.7% (range = 1.3–65.6%) and 31.4 ± 25.0% (range = 1.1–87.9%). The increase in tSNR was statistically significant using pipeline B compared to A, C compared to A, and C compared to B (two-tailed paired t-tests, all P values ≤ 1e−5), showing that using weighted averaging in addition to image registration provides further benefits compared to using image registration alone. These tSNR improvements relate to all scans in the data set, including scans with low movement during acquisition. If only ASL runs with a high amount of motion (ED >50 mm, i.e., ED >1 mm/vol on average) are considered, the tSNR further increases by 29.1 ± 15.8% (pipeline B) and 49.6 ± 24.3% (pipeline C). Statistically significant correlations were found between the ED in each scan and tSNR improvement in the corresponding PW time series after applying pipeline B ($R = 0.59$, $P = 4.6 \times 10^{-5}$) and after pipeline C ($R = 0.80$, $P = 2.3 \times 10^{-10}$) (see Supporting Information Figure S4).

The total ED averaged across runs (i.e., sum of ED for the 50 ASL tag/control volumes [25 ASL pairs] per patient), differed significantly between runs 1 and 2 (44.2 ± 17.3 mm vs. 61.4 ± 43.8 mm, two-tailed paired t-test, $P = 0.035$, data pooled from the 2 d) but not between d 1 and 2 (46.3 ± 20.7 mm vs. 54.8 ± 39.8 mm, two-tailed paired t-test, $P = 0.392$, data pooled from the 2 runs). This suggests that the likelihood of patient movement increases with the amount of time spent inside the scanner, and as such, particularly motion-sensitive sequences, such as ASL, should be acquired near the beginning of the scanning session.[46] A weak, albeit statistically significant negative correlation was found between patient age and ED ($R = -0.38$, $P = 0.014$). Furthermore, a statistically significant weak negative correlation was also found between the tSNR improvement and the patient age when comparing pipelines A and B ($R = -0.37$, $P = 0.015$) and A and C ($R = -0.49$, $P = 0.0009$), showing that these MC methods are especially useful in younger children.

ASL RBF estimates (complete pipeline)

RBF obtained across all scans of the entire pediatric cohort was 127.4 ± 81.8, 95.3 ± 46.9, and 94.7 ± 47.3 mL/100 g/min (mean ± SD), respectively using ASL pipelines A, B, and C. The effects of MC on the M_0, T_1, and RBF maps from an example run on 1 patient is shown in Figure 5. A single central slice is shown; because a single-shot 3D readout was used, all slices in the data set are motion-corrupted to the same extent. Images in Figures 5A–C show M_0 maps. Figure 5A and B were the output of SR fitting, respectively without and with MC; Figure 5C was obtained by a single PD-weighted acquisition. As such, it is largely immune to motion artefacts and can therefore serve as the "gold standard" to which the M_0 maps obtained by SR fitting can be compared. The reduction of artefacts in the M_0 map shown in Figure 5B compared to Figure 5A can be attributed to a reduction in SR fitting errors from an improved alignment of the kidneys in the SR time series following image registration. The greater similarity of Figure 5B compared to Figure 5C provides further evidence of the effectiveness of using mutual-information-based image registration to compensate for kidney displacements during the SR acquisition, despite intrinsic contrast changes because of varying post-saturation delays. Images in Figure 5E and F show whole-kidney T_1 maps, obtained respectively before and after MC, overlaid onto the PD image. The same T_1 information is shown, respectively in Figure 5I and J, but restricted to the voxels from which the mean T_1 estimates were obtained (excluding dilatations in the collecting system). Uncorrected renal movement gives rise to artefacts (e.g., lower pole of the kidney on the left side of Figure 5E). Image registration suppresses these as can be seen by comparing Figure 5E to F and Figure 5I to J. If these artefacts are left uncorrected, they result in severely inaccurate T_1 values that are then used for perfusion quantification, yielding erroneous RBF maps. MC reduces spurious variations in T_1 resulting in smoother T_1 maps with better anatomical specificity, preserving variations in T_1 values between different tissue types within the kidney (e.g., parenchyma vs. dilatations). Figure 5D shows clear PW signal in the regions of remaining functional parenchyma, no PW signal in the regions corresponding to the kidney dilatations, and no artefacts. Similar to when no MC was applied before SR fitting for T_1/M_0, artefacts are seen in the RBF maps close to the kidney boundaries if MC is not used (Figure 5G and K). If the averaged PWI is well motion-corrected (Figure 5D), the existence of such artefacts depends on the degree of alignment between the kidneys in the ASL and the "calibration" data (PD image and/or SR time series), which may change between different ASL runs and therefore directly influence the repeatability of the RBF measurements. The proposed MC approach not only improves the alignment of the individual control and/or label images in the ASL time series but also between the ASL data, the reference M_0 maps, and the T_1 maps obtained by SR fitting. Artefacts in the RBF maps are accordingly reduced (e.g., artefacts in the upper pole of both kidneys).

The results of the quantitative assessment of the repeatability of RBF obtained using the different processing pipelines are summarized in Table 3.

Image registration was particularly successful in improving the inter-session repeatability of the RBF estimates.

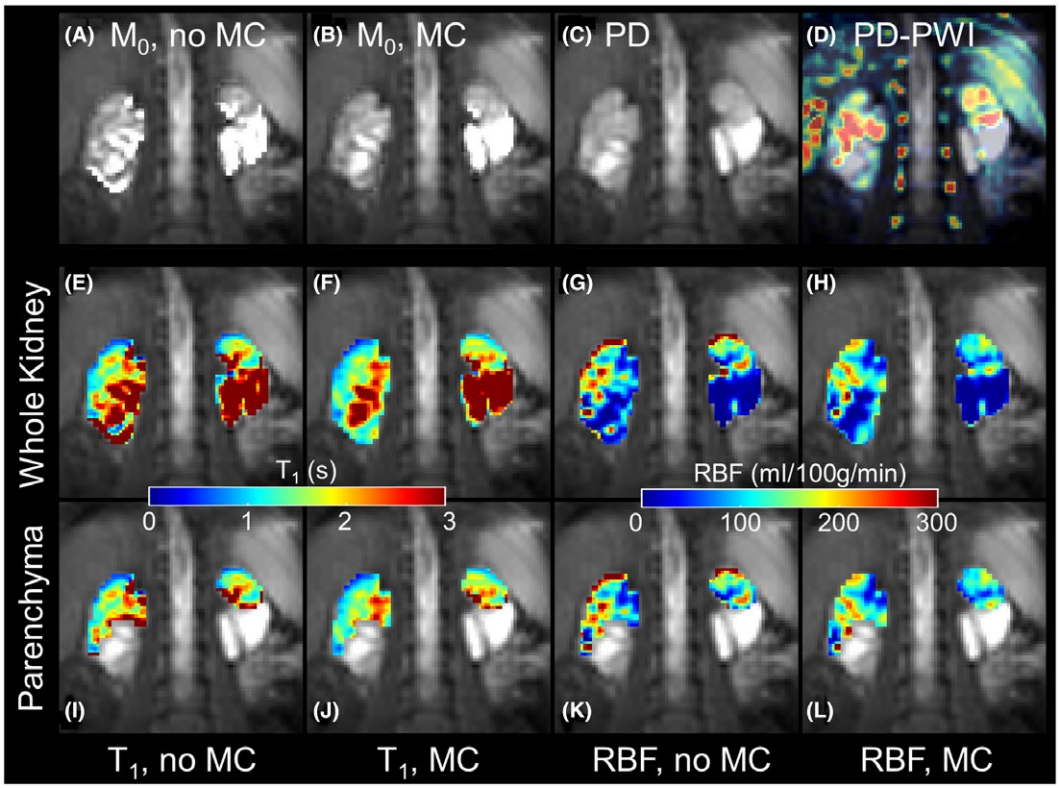

FIGURE 5 Effect of motion correction (MC) on the M_0, T_1, and RBF maps. (A) M_0 from SR fitting before MC. (B) M_0 from SR fitting after MC. (C) PD-weighted image (for ASL calibration). (D) PD-PWI fusion image (after MC) (see Supporting Information). (E) T_1 map before MC. (F) T_1 map after MC. (G) RBF map before MC. (H) RBF map after MC. (I–L) Same as (E)–(H) but T_1 and RBF only shown for functional renal parenchyma ROIs. The background anatomic data (grayscale) onto which all functional maps were superimposed corresponds to image (C)

TABLE 3 Intra-session and inter-session repeatability metrics for the mean cortical RBF estimates

	Intra-session repeatability			Inter-session repeatability		
Pipeline	**A**	**B**	**C**	**A**	**B**	**C**
	Pooled Days			**Pooled Runs**		
WSCV	0.145	0.186	0.179	0.506	0.201	0.204
ICC	0.936	0.857	0.873	0.372	0.833	0.834
	Day 1			**Run 1**		
WSCV	0.141	0.151	0.139	0.531	0.132	0.135
ICC	0.951	0.898	0.916	0.370	0.927	0.925
	Day 2			**Run 2**		
WSCV	0.149	0.218	0.214	0.453	0.282	0.285
ICC	0.853	0.818	0.834	0.329	0.645	0.657

Pipeline A, no motion correction; pipeline B, registration only; pipeline C, registration + weighted averaging; WSCV, within-subject coefficient of variation; ICC, intra-class correlation coefficient.
WSCV and ICC are color-coded so that red → green corresponds to worst → best.

Despite the prevalence of artefacts in the RBF maps without applying MC methods, the intra-session repeatability was high. Because both ASL runs shared the same M_0 (obtained from the same PD acquisition) systematic errors because of a consistent misalignment between the M_0 and the ASL data set in both ASL runs resulted in a repeatable mean RBF despite severe corruption in the RBF maps in the no-registration case. For this reason, intra-session WSCV and ICC alone should not be taken to be indicators of image quality directly. The lowest repeatability was found to be the inter-session repeatability of the second run of each day, which may reflect decreasing levels of compliance by the subjects the longer they remain in the scanner.

3.2.2 | Correlation of RBF and T_1

A statistically significant negative correlation was found between RBF and T_1 ($R = -0.57$, $P = 0.006$) in this patient cohort. This correlation reflects the fact that both T_1 and RBF are measures sensitive to pathology and supports the need for T_1 quantification on an individual subject basis to ensure accurate RBF quantification.

4 | DISCUSSION

Following a preliminary study to address the feasibility of renal ASL using single-shot 3D-GRASE in healthy

volunteers, we assessed RBF in a pediatric cohort with severe kidney disease (mean eGFR <30 mL/min per 1.73 m^2). This study is the first to report renal ASL repeatability metrics at such severe levels of kidney impairment (regardless of age), as well as in pediatric subjects (with our without CKD). Considering the challenging cohort (low perfusion SNR and high likelihood of movement), using MC methods improved the repeatability of our measurements enough to support the use of ASL for longitudinal assessment of changes in RBF, particularly if the conditions under which the ASL acquisition is performed are carefully chosen (e.g., at the beginning of the scanning session, with acquisition of the "calibration" data as close as possible to the actual ASL run). This study demonstrates the importance of a comprehensive retrospective MC pipeline, in which not only the main ASL time series is motion corrected but also all calibration data that directly feeds into the RBF quantification. Even though the use of weighted averaging improved the image quality of our ASL data, it did not further improve the repeatability of the RBF measurements. This may be because of the fact that the ASL protocol acquired a high number of ASL pairs (25 in the patient scans), making it inherently motion resilient, particularly when reporting quantitative MRI parameters from a ROI-based analysis. Outlier rejection may play a more significant role in ASL protocols with a reduced number of identical measurements (such as multi-TI ASL protocols) that are more motion-sensitive because of the inherently reduced number of ASL pairs acquired at each TI. Nevertheless, the fact that the proposed weighted averaging methods are fully automated (requiring only the optional use of masks to limit the regions over which the noise estimates are computed) and its application so far has not shown any negative effects on ASL data, regardless of the initial level of motion corruption, suggests that these can be readily implemented on renal ASL pipelines and may reduce the need for laborious manual image sorting when scanning challenging patient cohorts. Despite the known challenge of re-aligning background suppressed ASL data,[47] we have shown that image registration is capable of improving the tSNR of the PWI time series in our patient cohort, despite the low static tissue signal in the underlying ASL control and label images. Even though a TI = 1.2 s was used (the most common choice in renal pulsed ASL literature), the use of a single-TI may explain some of the RBF variability because of possible intravascular contributions or delays in the arrival of the ASL bolus in some subjects. The choice of performing a single-TI acquisition rather than a multi-TI acquisition was made to maximize scan speed, motion robustness, and PWI SNR in the pediatric cohort. Furthermore, partial volume effects are likely non-negligible given the chosen voxel size, which ultimately is linked to the trade-off of sensitivity (high SNR) and accuracy of the measurements (high resolution and therefore minimization of partial volume effects). This limitation may be addressed by using undersampling techniques that may allow, for example, an increase in spatial resolution while leaving the ETD unchanged.[48]

5 | CONCLUSIONS

We have presented a comprehensive retrospective motion-correction pipeline that addresses all stages of the ASL acquisition and processing procedure. We have shown the importance of registration of the separate volumes of a T_1 mapping SR acquisition to reduce errors in the SR fits, reduce artefacts, and improve the repeatability of the resulting T_1/M_0 maps that are used for ASL quantification. We have shown that automatic threshold-free weighted averaging methods can reduce the deleterious effects of corrupted PWIs. Furthermore, improving the alignment of the different sets of images required for ASL quantification allowed correction of an overestimation of RBF and greatly improved the repeatability of the ASL measurements in different scanning sessions. By applying these various methodological improvements, we have shown, for the first time, that renal ASL is feasible and robust in a pediatric cohort with severe kidney disease.

ACKNOWLEDGMENTS

This study was funded by Kidney Research UK (ST1/2013) and supported by the NIHR Great Ormond Street Hospital Biomedical Research Centre. DLT is supported by the UCL Leonard Wolfson Experimental Neurology Centre (PR/ylr/18575). We would also like to thank Prof. Matthias Günther for providing the 3D GRASE ASL pulse sequence.

REFERENCES

1. Detre JA, Leigh JS, Williams DS, Koretsky AP. Perfusion imaging. *Magn Reson Med*. 1992;23:37–45.
2. Williams DS, Detre JA, Leigh JS, Koretsky AP. Magnetic resonance imaging of perfusion using spin inversion of arterial water. *Proc Natl Acad Sci*. 1992;89:212–216.
3. Alsop DC, Detre JA, Golay X, et al. Recommended implementation of arterial spin-labeled perfusion MRI for clinical applications: a consensus of the ISMRM perfusion study group and the European consortium for ASL in dementia. *Magn Reson Med*. 2015;73:102–116.
4. Cox EF, Smith JK, Chowdhury AH, Lobo DN, Francis ST, Simpson J. Temporal assessment of pancreatic blood flow and perfusion following secretin stimulation using noninvasive MRI. *J Magn Reson Imaging*. 2015;42:1233–1240.
5. Kober F, Jao T, Troalen T, Nayak KS. Myocardial arterial spin labeling. *J Cardiovasc Magn Reson*. 2016;18:22. https://doi:10.1186/s12968-016-0235-4.
6. Shao X, Liu D, Martin T, et al. Measuring human placental blood flow with multidelay 3D GRASE pseudocontinuous arterial spin labeling at 3T. *J Magn Reson Imaging*. 2018;47:1667–1676.

7. Weller A, Barber JL, Olsen OE. Gadolinium and nephrogenic systemic fibrosis: an update. *Pediatr Nephrol*. 2014;29:1927–1937.
8. Rossi C, Artunc F, Martirosian P, Schlemmer HP, Schick F, Boss A. Histogram analysis of renal arterial spin labeling perfusion data reveals differences between volunteers and patients with mild chronic kidney disease. *Invest Radiol*. 2012;47:490–496.
9. Tan H, Koktzoglou I, Prasad PV. Renal perfusion imaging with two-dimensional navigator gated arterial spin labeling. *Magn Reson Med*. 2014;71:570–579.
10. Cai Y, Li Z, Zuo P, et al. Diagnostic value of renal perfusion in patients with chronic kidney disease using 3D arterial spin labeling. *J Magn Reson Imaging*. 2017;46:589–594.
11. Cox EF, Buchanan CE, Bradley CR, et al. Multiparametric renal magnetic resonance imaging: validation, interventions, and alterations in chronic kidney disease. *Front Physiol*. 2017;8:696.
12. Dong J, Yang L, Su T, et al. Quantitative assessment of acute kidney injury by noninvasive arterial spin labeling perfusion MRI: a pilot study. *Sci China Life Sci*. 2013;56:745–750.
13. Shimizu K, Kosaka N, Fujiwara Y, et al. Arterial transit time-corrected renal blood flow measurement with pulsed continuous arterial spin labeling MR imaging. *Magn Reson Med Sci*. 2017;16:38–44.
14. Hueper K, Gueler F, Bräsen JH, et al. Functional MRI detects perfusion impairment in renal allografts with delayed graft function. *Am J Physiol Renal Physiol*. 2015;308:F1444–F1451.
15. Ren T, Wen C-L, Chen L-H, et al. Evaluation of renal allografts function early after transplantation using intravoxel incoherent motion and arterial spin labeling MRI. *Magn Reson Imaging*. 2016;34:908–914.
16. Niles DJ, Artz NS, Djamali A, Sadowski EA, Grist TM, Fain SB. Longitudinal assessment of renal perfusion and oxygenation in transplant donor-recipient pairs using arterial spin labeling and blood oxygen level-dependent magnetic resonance imaging. *Invest Radiol*. 2016;51:113–120.
17. Cutajar M, Hilton R, Olsburgh J, et al. Renal blood flow using arterial spin labelling MRI and calculated filtration fraction in healthy adult kidney donors Pre-nephrectomy and post-nephrectomy. *Eur Radiol*. 2015;25:2390–2396.
18. Wang J, Zhang Y, Yang X, et al. Hemodynamic effects of furosemide on renal perfusion as evaluated by ASL-MRI. *Acad Radiol*. 2012;19:1194–1200.
19. Nery F, Gordon I, Thomas DL. Non-invasive renal perfusion imaging using arterial spin labeling MRI: challenges and opportunities. *Diagnostics (Basel)*. 2018;8.
20. Cutajar M, Thomas DL, Banks T, Clark CA, Golay X, Gordon I. Repeatability of renal arterial spin labelling MRI in healthy subjects. *MAGMA*. 2012;25:145–153.
21. Robson PM, Madhuranthakam AJ, Smith MP, et al. Volumetric arterial spin-labeled perfusion imaging of the kidneys with a three-dimensional fast spin echo acquisition. *Acad Radiol*. 2016;23:144–154.
22. Kim SG. Quantification of relative cerebral blood-flow change by flow-sensitive alternating inversion-recovery (FAIR) technique - application to functional mapping. *Magn Reson Med*. 1995;34:293–301.
23. Kwong KK, Chesler DA, Weisskoff RM, et al. MR perfusion studies with T1-weighted echo planar imaging. *Magn Reson Med*. 1995;34:878–887.
24. Luh WM, Wong EC, Bandettini PA, Hyde JS. QUIPSS II with thin-slice TI1 periodic saturation: a method for improving accuracy of quantitative perfusion imaging using pulsed arterial spin labeling. *Magn Reson Med*. 1999;41:1246–1254.
25. Günther M, Oshio K, Feinberg DA. Single-shot 3D imaging techniques improve arterial spin labeling perfusion measurements. *Magn Reson Med*. 2005;54:491–498.
26. De Vita E, Günther M, Golay X, Thomas DL. Magnetisation transfer effects of Q2TIPS pulses in ASL. *MAGMA*. 2012;25:113–126.
27. Ogg RJ, Kingsley PB, Taylor JS. WET, a T1- and B1-insensitive water-suppression method for in vivo localized 1H NMR spectroscopy. *J Magn Reson Ser B*. 1994;104:1–10.
28. Tan H, Maldjian JA, Pollock JM, et al. A fast, effective filtering method for improving clinical pulsed arterial spin labeling MRI. *J Magn Reson Imaging*. 2009;29:1134–1139.
29. Shirzadi Z, Crane DE, Robertson AD, et al. Automated removal of spurious intermediate cerebral blood flow volumes improves image quality among older patients: a clinical arterial spin labeling investigation. *J Magn Reson Imaging*. 2015;42:1377–1385.
30. Tanenbaum AB, Snyder AZ, Brier MR, Ances BM. A method for reducing the effects of motion contamination in arterial spin labeling magnetic resonance imaging. *J Cereb Blood Flow Metab*. 2015;35:1697–1702.
31. Atkinson D, Hill DL, Stoyle PN, Summers PE, Keevil SF. Automatic correction of motion artifacts in magnetic resonance images using an entropy focus criterion. *IEEE Trans Med Imaging*. 1997;16:903–910.
32. Breidthardt T, Cox EF, Squire I, et al. The pathophysiology of the chronic cardiorenal syndrome: a magnetic resonance imaging study. *Eur Radiol*. 2015;25:1684–1691.
33. Gillis KA, McComb C, Patel RK, et al. Non-contrast renal magnetic resonance imaging to assess perfusion and corticomedullary differentiation in health and chronic kidney disease. *Nephron*. 2016;133:183–192.
34. Gardener AG, Francis ST. Multislice perfusion of the kidneys using parallel imaging: Image acquisition and analysis strategies. *Magn Reson Med*. 2010;63:1627–1636.
35. Artz NS, Sadowski EA, Wentland AL, et al. Reproducibility of renal perfusion MR imaging in native and transplanted kidneys using non-contrast arterial spin labeling. *J Magn Reson Imaging*. 2011;33:1414–1421.
36. Marquez E, Sadowski E, Reese S, et al. Serum HSP27 is associated with medullary perfusion in kidney allografts. *J Nephrol*. 2012;25:1075–1080.
37. Song R, Tipirneni A, Johnson P, Loeffler RB, Hillenbrand CM. Evaluation of respiratory liver and kidney movements for MRI navigator gating. *J Magn Reson Imaging*. 2011;33:143–148.
38. Siva S, Pham D, Gill S, et al. An analysis of respiratory induced kidney motion on four-dimensional computed tomography and its implications for stereotactic kidney radiotherapy. *Radiat Oncol*. 2013;8:248.
39. Klein S, Staring M, Murphy K, Viergever MA, Pluim JP. elastix: a toolbox for intensity-based medical image registration. *IEEE Trans Med Imaging*. 2010;29:196–205.
40. Thévenaz P, Unser M, Thevenaz P. Optimization of mutual information for multiresolution image registration. *IEEE Trans Image Process*. 2000;9:2083–2099.
41. Klein S, Pluim JPW, Staring M, Viergever MA. Adaptive stochastic gradient descent optimisation for image registration. *Int J Comput Vis*. 2009;81:227–239.

42. Studler U, White LM, Andreisek G, Luu S, Cheng HL, Sussman MS. Impact of motion on T1 mapping acquired with inversion recovery fast spin echo and rapid spoiled gradient recalled-echo pulse sequences for delayed gadolinium-enhanced MRI of cartilage (dGEMRIC) in volunteers. *J Magn Reson Imaging*. 2010;32:394–398.
43. Song R, Loeffler RB, Hillenbrand CM. Improved renal perfusion measurement with a dual navigator-gated Q2TIPS fair technique. *Magn Reson Med*. 2010;64:1352–1359.
44. de Bazelaire CM, Duhamel GD, Rofsky NM, Alsop DC. MR imaging relaxation times of abdominal and pelvic tissues measured in vivo at 3.0 T: preliminary results. *Radiology*. 2004;230:652–659.
45. Artz NS, Sadowski EA, Wentland AL, et al. Arterial spin labeling MRI for assessment of perfusion in native and transplanted kidneys. *Magn Reson Imaging*. 2011;29:74–82.
46. Cahoon G. Techniques in pediatric MRI - tips for imaging children. *MAGNETOM Flash*. 2011;2:6–16.
47. Cutajar M, Thomas DL, Hales PW, Banks T, Clark CA, Gordon I. Comparison of ASL and DCE MRI for the non-invasive measurement of renal blood flow: quantification and reproducibility. *Eur Radiol*. 2014;24:1300–1308.
48. Griswold MA, Jakob PM, Chen Q, et al. Resolution enhancement in single-shot imaging using simultaneous acquisition of spatial harmonics (SMASH). *Magn Reson Med*. 1999;41:1236–1245.

SUPPORTING INFORMATION

Additional supporting information may be found online in the Supporting Information section at the end of the article.

Figure S1 Averaged PWIs obtained with and without applying the $wMean_{masked}^{MVARS}$ method

Figure S2 Averaged PWIs and voxelwise tSNR maps before and/or after noise-correction using $wMean_{masked}^{MVARS}$ (data from all healthy volunteers). Column A: mean PWI before correction. Column B: mean PWI after correction. Column C: voxelwise tSNR map before correction. Column D: voxelwise tSNR map after correction. The values in tSNR maps correspond to the mean increase in this metric in the cortical ROI when compared to the "No correction" case

Figure S3 Effect of using $wMean_{masked}^{MVARS}$ on the contribution of each PWI (before averaging) to the mean PWI (subject 1). Top: individual PWIs (before averaging). Table: weights attributed to each individual PWI by $wMean_{masked}^{MVARS}$ (convergence reached by iteration 3)

Figure S4 Improvement in tSNR after applying the proposed motion correction (MC) pipelines. The scatter plot displays the percent increase (i.e., improvement) in tSNR in the PWI time series after applying the MC processing pipelines B and C relative to the "no MC" case (pipeline A) plotted against the amount of renal translation motion, for each individual ASL run ($N = 42$). Linear regression lines as well as the Pearson correlation coefficient (R) and P values are shown

How to cite this article: Nery F, De Vita E, Clark CA, Gordon I, Thomas DL. Robust kidney perfusion mapping in pediatric chronic kidney disease using single-shot 3D-GRASE ASL with optimized retrospective motion correction. *Magn Reson Med*. 2018;00:1–13. https://doi.org/10.1002/mrm.27614